1. Analytical treatment of Adiabatic Fast Passage

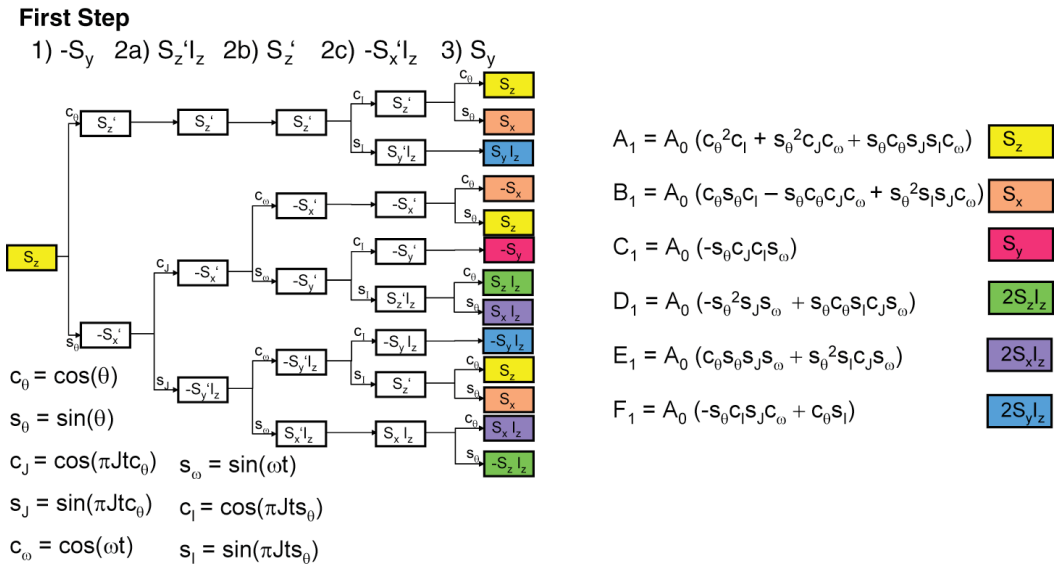

Figure S1: Starting out with longitudinal magnetization with intensity A_0, the rotating frame Hamiltonian is tilted by an angle θ into the spin-lock frame (step 1), where coherent evolution (Larmor precession and scalar coupling in the tilted frame) takes place (steps 2a, 2b, 2c); in a final step (3), operators are returned to the rotating frame. Thus, the manifold of six operators that span the relevant magnetization subspace is created. Their relative contributions to the total magnetization are indicated as A_1 to F_1.

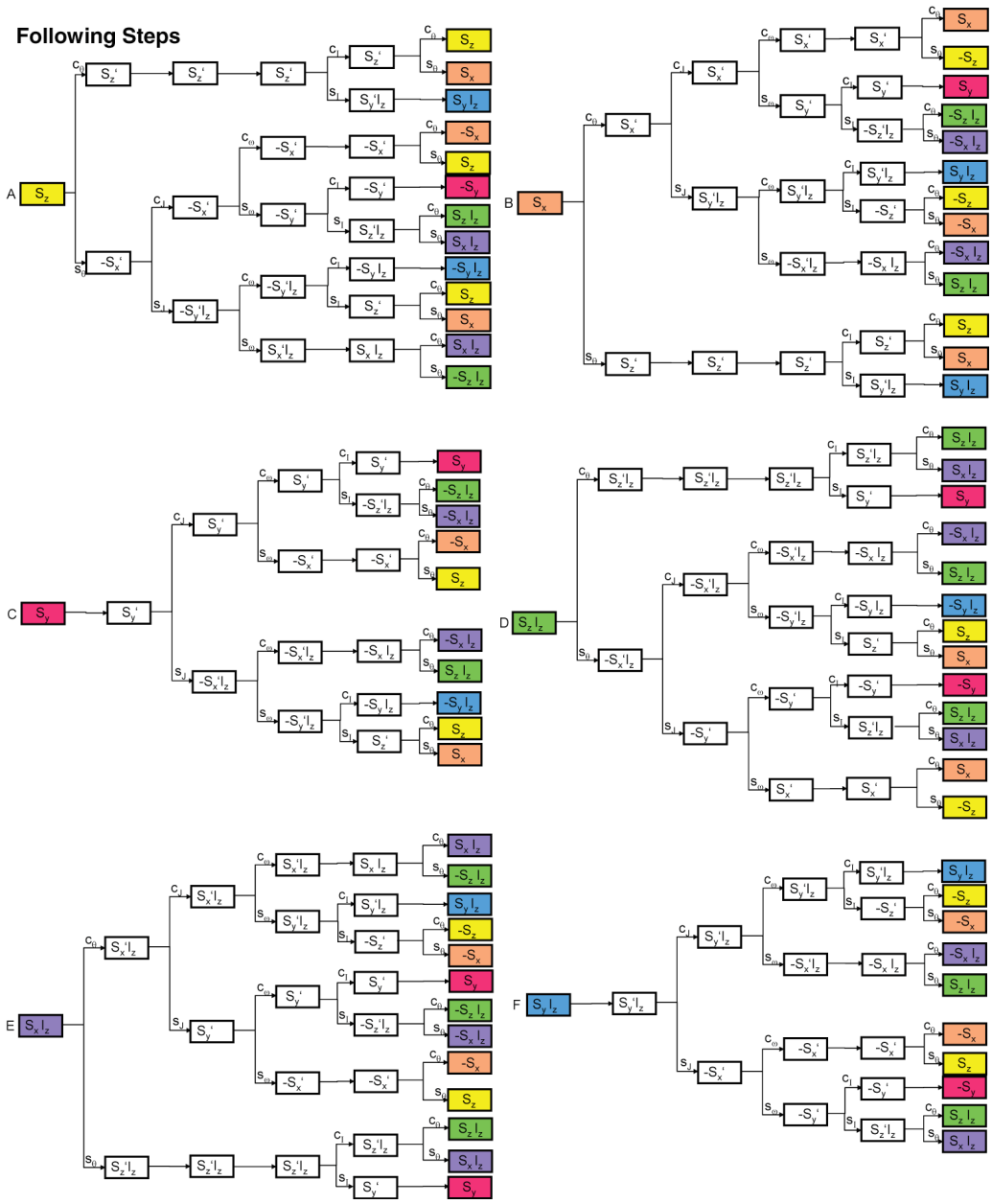

Figure S2: In all following steps, this procedure is performed for each of the six operators.

The resulting evolution is summarized in table S1. Note that the computation is carried out for very small time-steps, and that after each time-step t, it is necessary to account for non-coherent evolution (auto- and cross-correlated relaxation, as well as conformational exchange, see also main text).

	S_z A_i	S_x B_i	S_y C_i	$S_z I_z$ D_i	$S_x I_z$ E_i	$S_y I_z$ F_i
S_z A_{i+1}	$C_\theta^2C_I + S_\theta^2C_JC_\omega + S_\theta C_\theta S_I S_J C_\omega$	$C_\theta S_\theta C_I - C_\theta S_\theta C_J C_\omega - C_\theta^2 S_I S_J C_\omega$	$S_\theta C_J S_\omega + C_\theta S_I S_J S_\omega$	$-S_\theta^2 S_J S_\omega + C_\theta S_\theta S_I C_J S_\omega$	$C_\theta S_\theta S_J S_\omega - C_\theta^2 S_I C_J S_\omega$	$S_\theta S_J C_\omega - C_\theta S_I C_J C_\omega$
S_x B_{i+1}	$C_\theta S_\theta C_I - C_\theta S_\theta C_J C_\omega + S_\theta^2 S_I S_J C_\omega$	$C_\theta^2 C_J C_\omega + S_\theta^2 C_I - C_\theta S_\theta S_I S_J C_\omega$	$-C_\theta C_J S_\omega + S_\theta S_I S_J S_\omega$	$C_\theta S_\theta S_J S_\omega + S_\theta^2 S_I C_J S_\omega$	$-C_\theta^2 S_J S_\omega - S_\theta C_\theta S_I C_J S_\omega$	$-C_\theta S_J C_\omega - S_\theta S_I C_J C_\omega$
S_y C_{i+1}	$-S_\theta C_I C_J S_\omega$	$C_\theta C_I C_J S_\omega$	$C_I C_J C_\omega$	$-S_\theta C_I S_J C_\omega + C_\theta S_I$	$C_\theta C_I S_J C_\omega + S_\theta S_I$	$-C_I S_J S_\omega$
$S_z I_z$ D_{i+1}	$-S_\theta^2 S_J S_\omega + S_\theta C_\theta S_I C_J S_\omega$	$C_\theta S_\theta S_J S_\omega - C_\theta^2 C_J S_I S_\omega$	$S_\theta S_J C_\omega - C_\theta S_I C_J C_\omega$	$C_\theta^2 C_I + S_\theta^2 C_J C_\omega + C_\theta S_\theta S_I S_J C_\omega$	$C_\theta S_\theta C_I - C_\theta S_\theta C_J C_\omega - C_\theta^2 S_I S_J C_\omega$	$S_\theta C_J S_\omega + C_\theta S_I S_J S_\omega$
$S_x I_z$ E_{i+1}	$C_\theta S_\theta S_J S_\omega + S_\theta^2 S_I C_J S_\omega$	$-C_\theta^2 S_J S_\omega - C_\theta S_\theta S_I C_J S_\omega$	$-C_\theta S_J C_\omega - S_\theta S_I C_J C_\omega$	$C_\theta S_\theta C_I - C_\theta S_\theta C_J C_\omega + S_\theta^2 S_I S_J C_\omega$	$C_\theta^2 C_J C_\omega + S_\theta^2 C_I - S_\theta C_\theta S_I S_J C_\omega$	$-C_\theta C_J S_\omega + S_\theta S_I S_J S_\omega$
$S_y I_z$ F_{i+1}	$-S_\theta C_I S_J C_\omega + C_\theta S_I$	$C_\theta C_I S_J C_\omega + S_\theta S_I$	$-C_I S_J S_\omega$	$-S_\theta C_I C_J S_\omega$	$C_\theta C_I C_J S_\omega$	$C_I C_J C_\omega$

Table S1: Resulting modulation of the six operators that span the subspace relevant for evolution during spinlock conditions. The table is read from top to bottom - for example, starting out from one of the operators in the first row, it is converted into a combination of the six operators, given in the pertinent column.

2. Experiments

The spinlock relaxation rate consists of longitudinal and transverse parts, and in theory, R_1 and R_2 can be obtained directly from $R_{1\rho}(\sin^2\theta_{eff})$ (by extrapolation to $\sin^2\theta_{eff}=0$ and $\sin^2\theta_{eff}=1$, respectively) *in the absence of chemical exchange*, as exemplified in Konrat et al. (Konrat and Tollinger 1999). In practice, however, R_1 was poorly determined due to the violation of the adiabatic condition at low spinlock field strengths (see the spikes in figure S3) and had to be obtained from a separate measurement. R_2 on the other hand was well-characterized by the slope of the linear dependence of $R_{1\rho}$ on $\sin^2\theta_{eff}$.

For analyzing $R_{1\rho}$ relaxation rates in systems with modulation of the isotropic chemical shift, it is also necessary to record a reference experiment measuring R_1. Here, we additionally determined exchange-free transverse relaxation rates from measurement of cross-correlated relaxation rates (Tessari, Vis et al. 1997; Tjandra and Bax 1997; Pelupessy, Espallargas et al. 2003). In addition, inclusion of CSA-DD cross-correlated relaxation rates into the computation is necessary in order not to compromise the accuracy of the calculation (see main text).

To experimentally demonstrate the effect of exchange contributions to adiabatic fast passage relaxation experiments, measurements were performed on the KIX domain of the CBP protein (results shown in Figure S3). KIX is a 91-residue (11kDa) KID (kinase-inducible domain) binding domain of CREB-binding protein involved in gene transcription (Radhakrishnan, Perez-Alvarado et al. 1997). KIX exchanges under native conditions between a highly populated folded state consisting of three α-

helices and a high-energy, partially unfolded state, in which residual helical structure is retained to a variable degree in two helices while the rest of the protein is devoid of any residual secondary structure elements (Tollinger, Kloiber et al. 2006).

As expected for a system with millisecond motion, significant deviations from linearity can be seen in the plot of $R_{1\rho}$ *vs* $\sin^2\theta_{eff}$. For comparison and to demonstrate the quality of the experimental data, the expected rates were computed on the basis of the exchange parameters obtained from ^{15}N CPMG relaxation dispersion experiments (Tollinger, Kloiber et al. 2006), longitudinal and exchange-free transverse relaxation rates, and CSA-DD cross-correlated relaxation rates. Theoretical predictions and experimental data agree very well thus pointing to the reliability of the proposed methodology.

Figure S3 also shows the quenching efficiency of the adiabatic spin-lock field as a function of sweep range (ν_{sweep}). One consequence of a larger sweep range is that magnetization remains longitudinal for a larger fraction of the pulse. Thus a larger spinlock amplitude is necessary in order to *reach* a particular $\sin^2\theta_{eff}$ (for instance, an rf field of about 1000Hz results in $\sin^2\theta_{eff}$ of approx. 0.45 for ν_{sweep}=5000Hz and 0.8 for ν_{sweep}=1000Hz). This affects the relative weights of longitudinal and transverse relaxation at a given spinlock field: for larger sweep widths, the transverse component is smaller than for smaller ones, scaling down the exchange contribution which is picked up at this particular field. At the same time, larger effective field strengths are realized in wider sweeps, also leading to increased quench efficiency. This results in a less prominent deviation from the exchange free value at a given $\sin^2\theta_{eff}$.

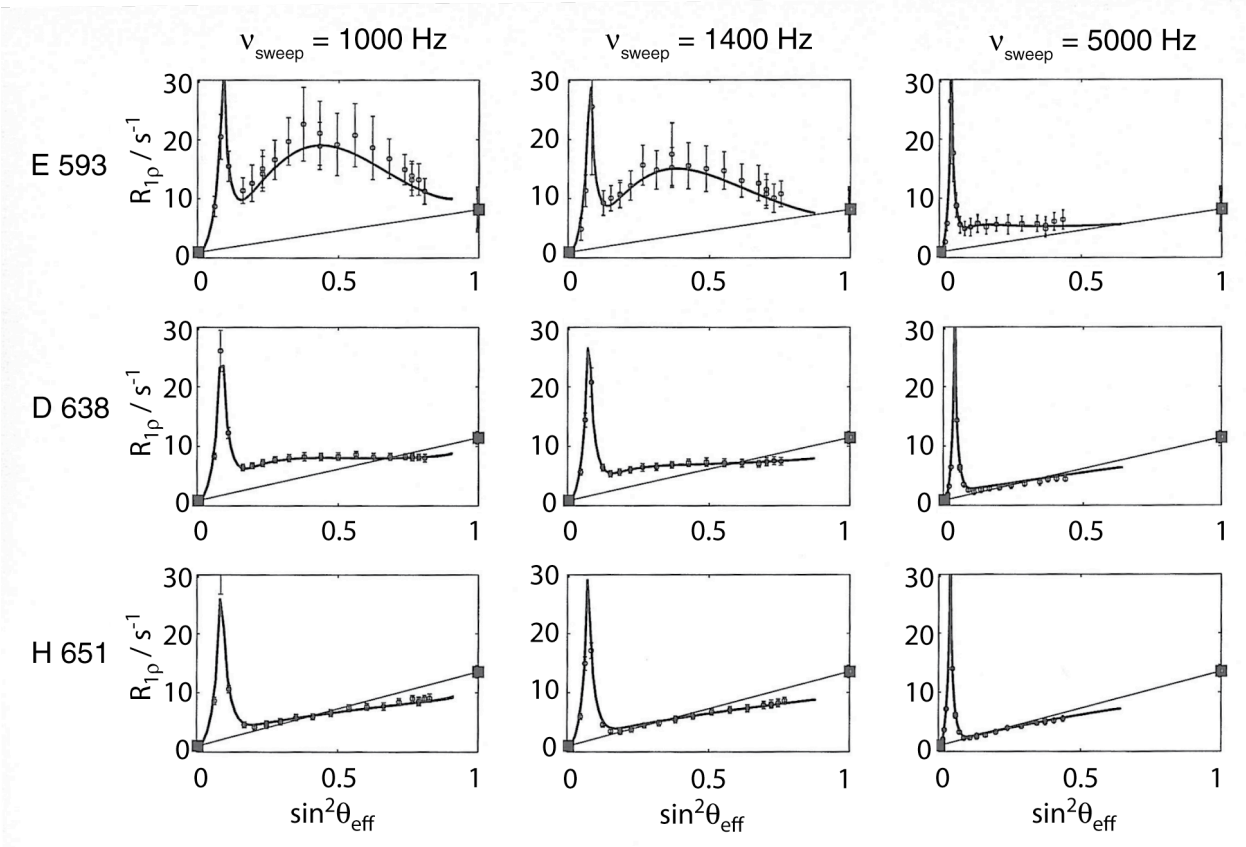

Figure S3. AFP profiles $R_{1\rho}$ *vs* $\sin^2\theta_{eff}$ at 18.8T of the KIX residues E593, D638 and H651 (top to bottom). The frequency of the adiabatic pulse is swept linearly over 1000Hz (left), 1400 (middle) and 5000Hz (right). The straight line represents an isolated spin according to $R_{1\rho} = R_1 + (R_2 - R_1) \sin^2\theta_{eff}$ assuming exchange-free R_2. R_1 ($R_{1\rho}$ at $\sin^2\theta_{eff}$=0) and exchange-free R_2^0 ($R_{1\rho}$ at $\sin^2\theta_{eff}$=1) were gained from separate measurements: R_1 from conventional inversion recovery (Farrow, Muhandiram et al. 1994) and R_2^0 from CSA-DD cross correlation experiments (Pelupessy, Espallargas et al. 2003). The spike on the left hand side is a consequence of the violation of the adiabaticity condition (e.g. imperfect inversion). Exchange parameters were k_{ex} = 876 s^{-1}, p_B = 3.8%. $\Delta\omega$ was 4.79, 1.80, and 0.49 ppm for residues E593, D638, H651, respectively. From the left to the right, the deviation from the straight line becomes less pronounced as the AFP sweep width is increased.

3. Synthetic data sets

We have generated synthetic data sets using the following parameters for the AFP pulse: duration t_{AFP} = 0.1 s; number of steps = 2500; sweep width = 2000 Hz, ramping = 20% on each side. Exchange parameters were p_b=0.2, $\Delta\omega$=3 ppm, R_2(11.7T)=10 s^{-1}, and R_2(18.8T)=13 s^{-1}; k_{ex} was set to 800, 3000, and 10000 s^{-1}, respectively ($\log(k_{ex}/\Delta\omega)$ = -0.07, 0.50, 1.02). It has been assumed that CSA-DD cross-correlated relaxation has been accounted for. 11x2 data points were computed (2 field strengths, 11 spin lock amplitudes, see main text) and randomized using different standard deviations for the rates (0.25 -2 s^{-1}) ('R_{exp}'). A two-state exchange model (fit parameters k_{ex}, p_b, $\Delta\omega$, R_2(11.7T), and R_2(18.8T)) was fit to the data once using the Trott-Palmer equation for computing magnetization for every step in the AFP trajectory. The minimization parameter was $\chi^2 = \sqrt{\left(R_{exp} - R_{fit}\right)^2 / np}$, where the number of data points np was 22. In a Monte Carlo procedure, the resulting fitted rates ('R_{fit}') were randomized and fit 200 times (also initial conditions were randomized in every step in order to access eventual further minima[1]), giving rise to the scatter plots and the ensembles of fitted AFP profiles shown in figures S4a-S4e. In figures S4a-S4c results for the three different exchange rate constants are shown for experimental errors corresponding to a standard deviation in rates of 0.25s-1. Figure S4d and S4c show the influence of experimental errors on the statistics for S4b and S4c.

[1] range of variations of initial conditions around the first fit results:
0.3 k_{ex}^{fit} [s^{-1}], 0.05*p_b^{fit}, 1 [ppm], 3 [s^{-1}], 3 [s^{-1}]

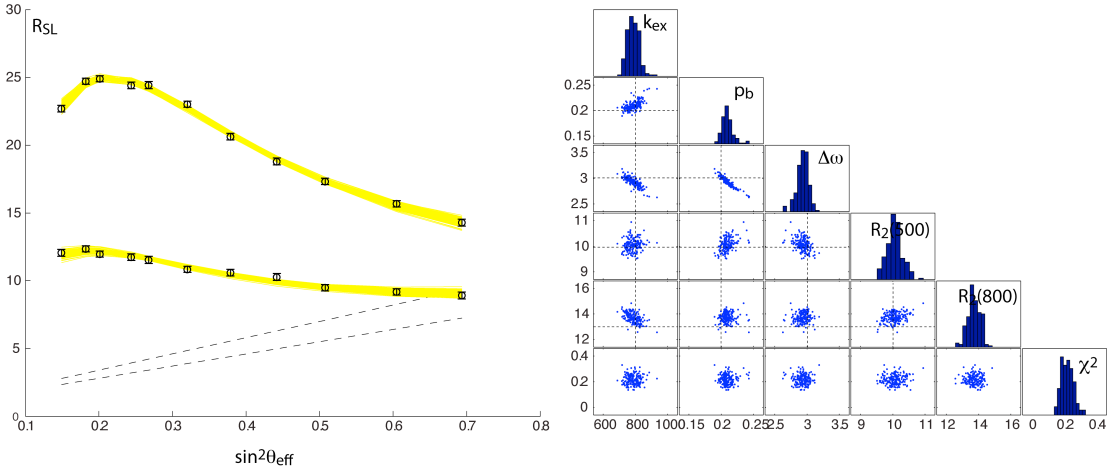

Figure S4a. Fits and scatter plots for k_{ex}=800s^{-1}. 'R_{exp}' as a function of $\sin^2\theta_{eff}$ is shown as black circles with errorbars, the fits ('R_{fit}') are shown as an ensemble of yellow lines. Black dashed lines are the spinlock rates in the absence of conformational exchange. Standard deviation in experimental spin lock rates was assumed to be 0.25 s^{-1}. Correct parameters are shown in the scatter plots as intersections of dashed lines.

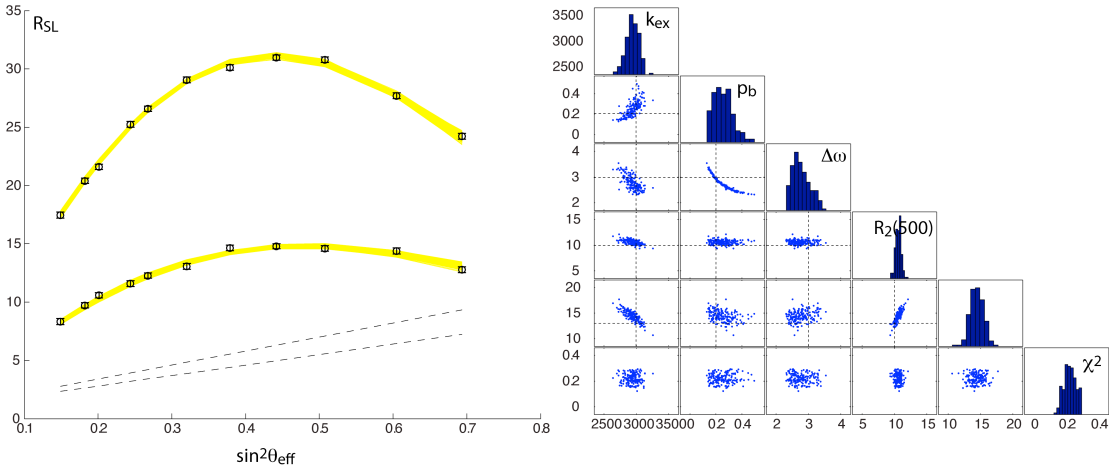

Figure S4b. Fits and scatter plots for k_{ex}=3000s^{-1}. 'R_{exp}' as a function of $\sin^2\theta_{eff}$ is shown as black circles with errorbars, the fits ('R_{fit}') are shown as an ensemble of yellow lines. Black dashed lines are the spinlock rates in the absence of conformational exchange. Standard deviation in experimental spin lock rates was assumed to be 0.25 s^{-1}. Correct parameters are shown in the scatter plots as intersections of dashed lines.

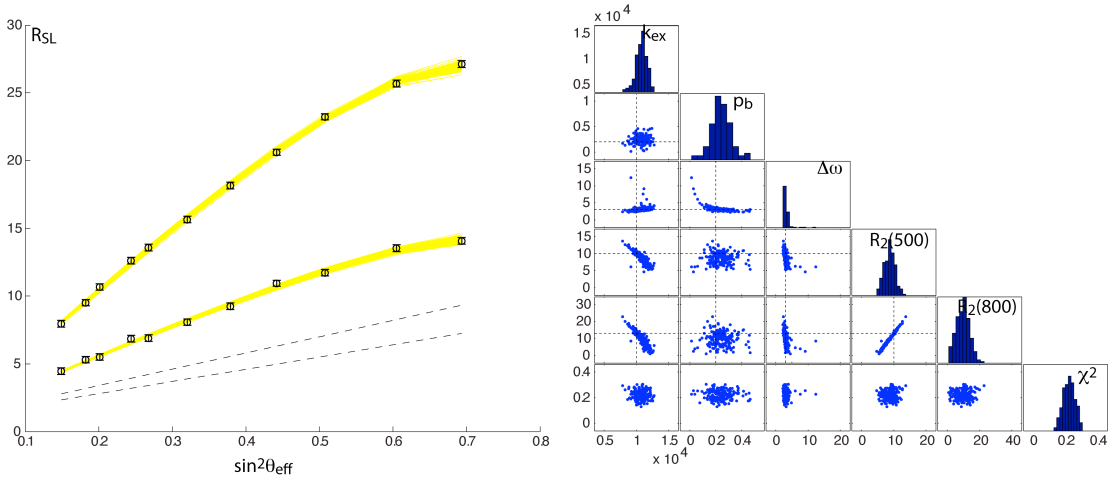

Figure S4c. Fits and scatter plots for k_{ex}=10000s^{-1}. 'R_{exp}' as a function of $\sin^2\theta_{eff}$ is shown as black circles with errorbars, the fits ('R_{fit}') are shown as an ensemble of yellow lines. Black dashed lines are the spinlock rates in the absence of conformational exchange. Standard deviation in rates was assumed 0.25s^{-1}. Negative k_{ex}, R_2(500) and R_2(800) were omitted from the plot. Correct parameters are shown as intersections of dashed lines in the scatter plots.

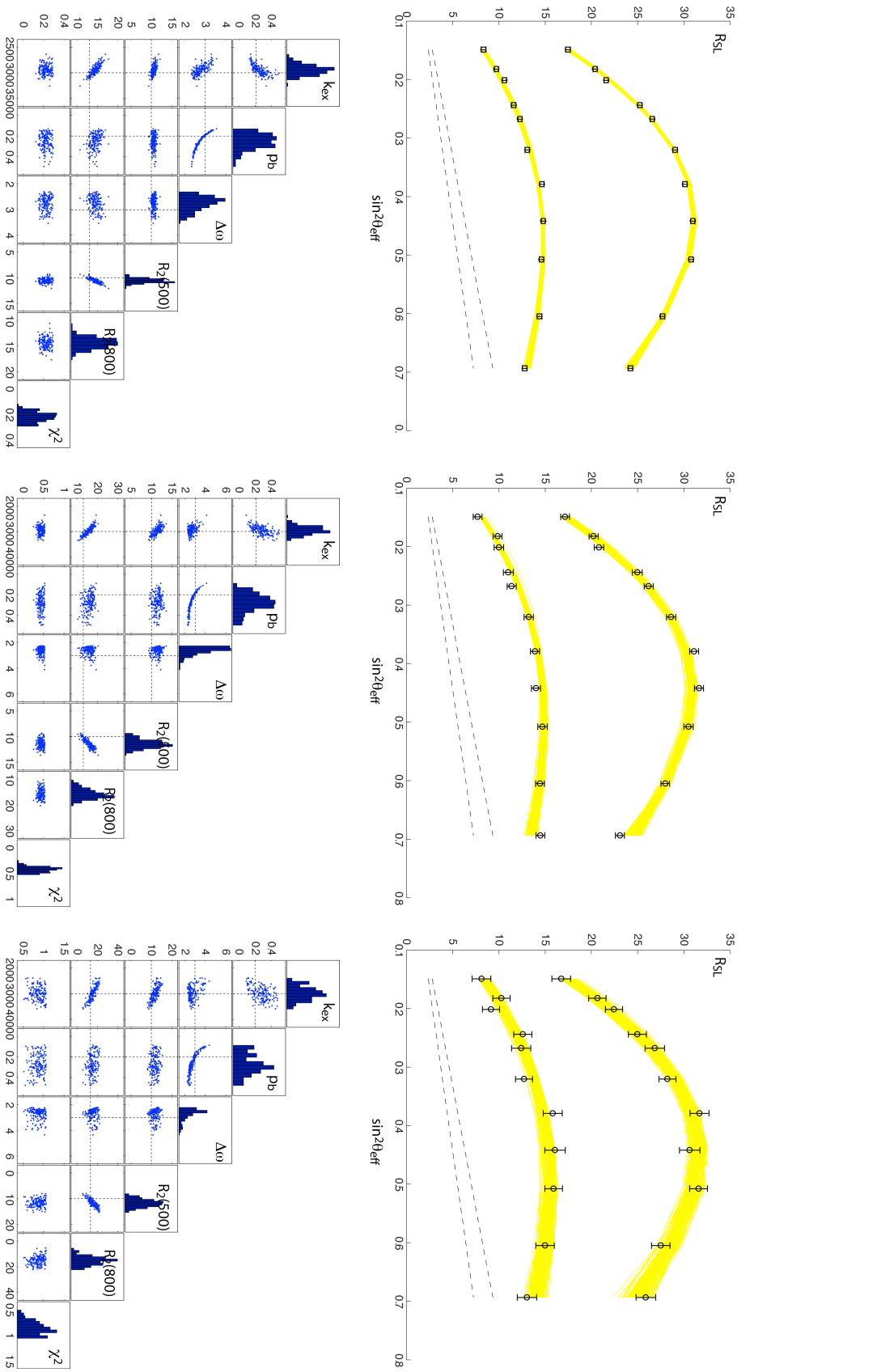

Figure S4d: Fits and scatter plots for k_{ex}=3000s^{-1}, with different experimental errors: Leftmost panel: dR = 0.25s^{-1}, middle panel: dR =0.5s^{-1}, right panel: dR = 1s^{-1} (dR is the standard deviation).

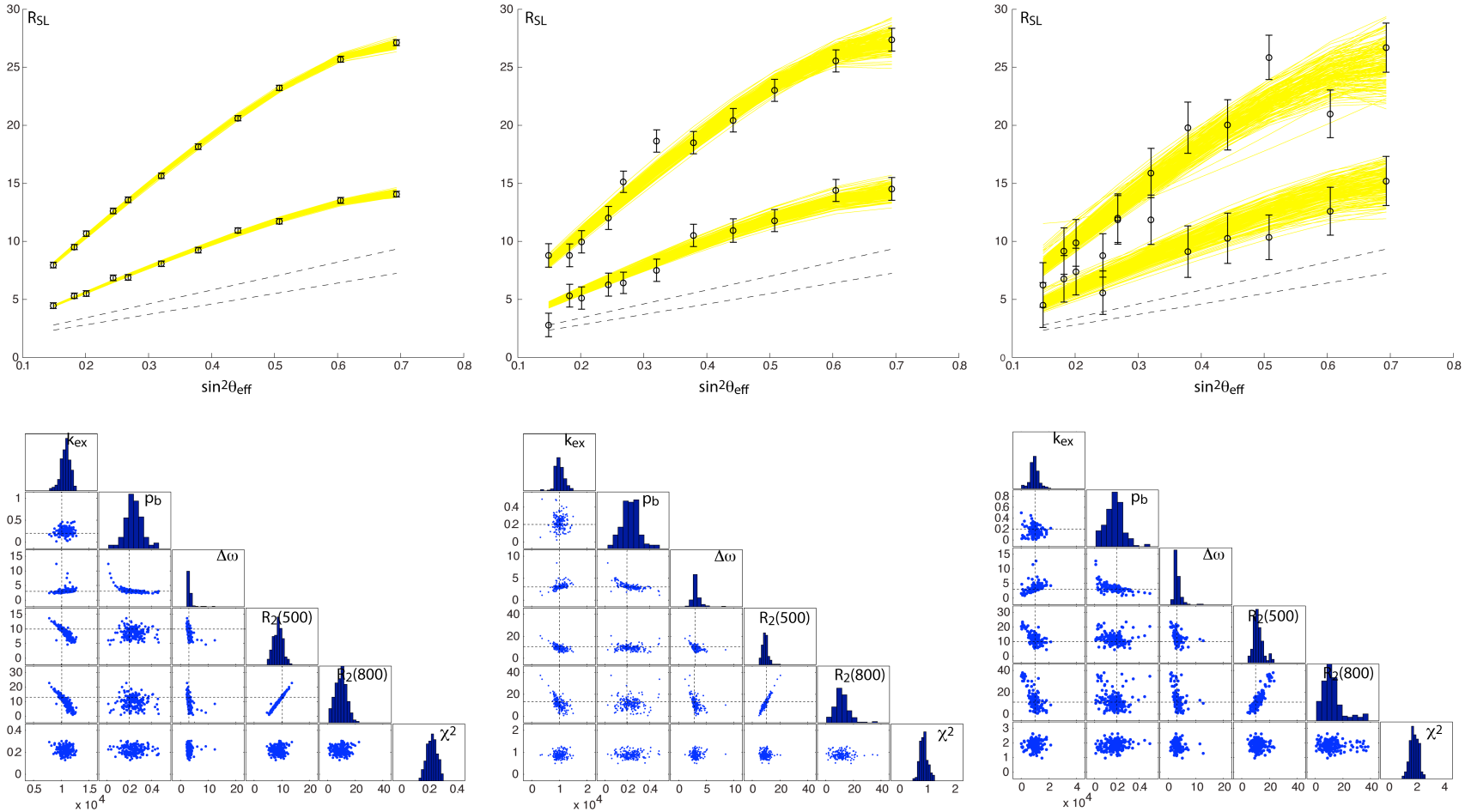
RSL
sin2θeff
kex
pb
Δω
R2(500)
R2(800)
χ2
x 10^4

Figure S4e: Fits and scatter plots for $k_{ex}=10000s^{-1}$, with different experimental errors: Leftmost panel: dR = $0.25s^{-1}$, middle panel: dR = $1s^{-1}$, right panel: dR = $2s^{-1}$ (dR is the standard deviation).

Farrow, N. A., R. Muhandiram, et al. (1994). "Backbone dynamics of a free and phosphopeptide-complexed Src homology 2 domain studied by 15N NMR relaxation." Biochemistry **33**(19): 5984-6003.

Konrat, R. and M. Tollinger (1999). "Heteronuclear relaxation in time-dependent spin systems: (15)N-T1 (rho) dispersion during adiabatic fast passage." J Biomol NMR **13**(3): 213-221.

Pelupessy, P., G. M. Espallargas, et al. (2003). "Symmetrical reconversion: measuring cross-correlation rates with enhanced accuracy." J Magn Reson **161**(2): 258-264.

Radhakrishnan, I., G. C. Perez-Alvarado, et al. (1997). "Solution structure of the KIX domain of CBP bound to the transactivation domain of CREB: a model for activator:coactivator interactions." Cell **91**(6): 741-752.

Tessari, M., H. Vis, et al. (1997). "Quantitative Measurement of Relaxation Interference Effects between 1HN CSA and 1H-15N Dipolar Interaction: Correlation with Secondary Structure." J Am Chem Soc **119**: 8985-8990.

Tjandra, N. and A. Bax (1997). "Solution NMR Measurement of Amide Proton Chemical Shift Anisotropy in 15N-Enriched Proteins. Correlation with Hydrogen Bond Length." J Am Chem Soc **119**: 8076-8082.

Tollinger, M., K. Kloiber, et al. (2006). "An isolated helix persists in a sparsely populated form of KIX under native conditions." Biochemistry **45**(29): 8885-8893.